Article:

Poluri, N. and De Souza, M.M. orcid.org/0000-0002-7804-7154 (2018) Investigation of the effect of weak non-linearities on P1dB and efficiency of class B/J/J* amplifiers. IEEE Transactions on Circuits and Systems II: Express Briefs, 65 (9). pp. 1159-1163. ISSN 1549-7747

https://doi.org/10.1109/TCSII.2018.2810944

Investigation of the Effect of Weak Non-Linearities on P1dB and Efficiency of Class B/J/J* Amplifiers

Nagaditya Poluri and Maria Merlyne De Souza, *Member, IEEE*

***Abstract*—The variation of phase of the current through the non-linear intrinsic capacitances of a high-power RF device caused by the variation of the phase in the continuum of drain voltage waveforms in Class B/J/J* leads to a reduction of intrinsic drain current when moving from class B to class J* while the drain current increases from class B to class J. Consequently, a subset of voltage waveforms of the class B/J/J* continuum can be used to design amplifiers with higher P1dB, and efficiency at P1dB than in Class B. A simple choice of this subset is demonstrated with a 2.6GHz Class B/J/J* amplifier, achieving a P1dB of 38.1dBm and PAE at P1dB of 54.7%, the highest output power and efficiency at P1dB amongst narrowband linear amplifiers using the CGH40010 reported to date, at a comparable peak PAE of 72%.**

***Index Terms*—Class B/J/J* continuum, non-linear capacitances, Power amplifier, GaN HEMT, linearity, IMD3**

I. Introduction

Wireless communication systems require power amplifiers with high efficiency and linearity to reduce battery consumption and interference respectively. As a solution, Cripps et. al. [1] proposed a continuum of voltage waveforms from class J*/B/J, which differ in phase, but achieve constant output power and peak efficiency. These high efficiency, yet linear, waveforms require inductive, short, and capacitive loads for classes J*, B and J, respectively, at the second harmonic, whilst the reactive component of the fundamental load is adjusted according to the load impedance at the second harmonic. The principle of class B/J/J* continuum has been applied to classes E, F, and F^{-1} to alleviate the need for precise load terminations with the resulting modes referred to as continuous classes E [2], F[3], and F^{-1}[4] respectively. The continuum modes demonstrate efficiency above 60% over a wide bandwidth [3]–[7] and allow the drain capacitance to be absorbed into the output matching network thus easing amplifier design [7].

Interestingly, the class B/J/J* continuum and the continuous class F demonstrate state-of-the-art high efficiencies at P1dB and at back-off power levels, as summarized in Table I. It appears that the improvement of efficiency at back-off in Class B/J/J* can be attributed to the current generated from intrinsic capacitances. For the case of class J, the improvement over class B is due to the harmonics of current generated from the non-linear output capacitance C_{out} (a combination of the feedback capacitance (C_{gd}) and drain-source capacitance (C_{ds})) [8].

Manuscript received September 28, 2017; revised December 20, 2017; accepted February 1, 2018. This work was supported by ENIAC-JU project PARSIMO under Grant 270687. This brief was recommended by Associate Editor D. D.-C. Lu. *(Corresponding authors: Nagaditya Poluri and Maria Merlyne De Souza.)*

TABLE I

Reported High Efficiencies at P1dB and Back-off Power

Ref.	Mode	Device Technology	Psat (dBm)	Merit	Freq. (in GHz)
[9]	Class B/J/J*	GaAs pHEMT	27.4	62% PAE at P1dB	5.25
[10]	Class B/J/J*	GaN HEMT	39.7	50% DE at 5dB backoff	2.13
[11]	Class B/J/J*	GaN HEMT	41.2	50% DE at 5.5dB backoff	2.5
[12]	Class B/J/J*	GaN HFET	26.8	44% PAE at10dB backoff	2.5
[13]	CCF	GaN HEMT	42.2	42% DE at 6.5dB backoff	2.14

DE and **PAE** denote Drain Efficiency and Power Added Efficiency respectively. **CCF** denotes Continuous class F. **Freq.** denotes Frequency.

The harmonics from non-linear C_{out} have been shown to improve peak PAE in continuous class F[13].

However, no work, to date, has described conditions to obtain high efficiencies at P1dB and back-off power nor has analysed the influence of the weak non-linearities (non-linear gm and non-linear capacitances) on the performance of a class B/J/J* amplifier, as addressed in this work. A simple method that relies on an analysis of weak non-linearities on the intrinsic drain current is illustrated for the selection of high-efficiency voltage waveforms in the continuum.

II. Effect of Weak Non-Linearities

The device selected for this study is a 10W GaN HEMT, CGH40010F, biased in deep class AB mode (V_{dsq}=28V, I_{dsq}=150mA) with an optimal loadline resistance (R_L) of 38.1Ω. The equivalent circuit of the transistor used for our analysis using ADS is shown in Fig. 1. The values of the extrinsic parasitic elements and intrinsic capacitors of the device are extracted from the from the Z and Y parameters vendor model using the algorithms presented in [14] and [15] respectively. The non-linear current generator I_{gen} is implemented via a table look-up as a function of the intrinsic gate (V_{gsi}) and drain (V_{dsi}) voltages. Analysis of the Intermodulation products and ACPR is undertaken using the vendor model.

A. Influence of Intrinsic Parasitic Elements on the Intrinsic Drain current

The influence of the intrinsic capacitances on the drain current is analyzed by dividing the intrinsic device into resistive and capacitive cores [16] as shown in Fig. 1. The currents in the

The authors are with the Department of Electrical and Electronics Engineering, University of Sheffield, Sheffield S37HQ, U.K. (e-mail: npoluri1@sheffield.ac.uk; m.desouza@sheffield.ac.uk).

Color versions of one or more of the figures in this paper are available online at http://ieeexplore.ieee.org.

Digital Object Identifier 10.1109/TCSII.2018.2810944

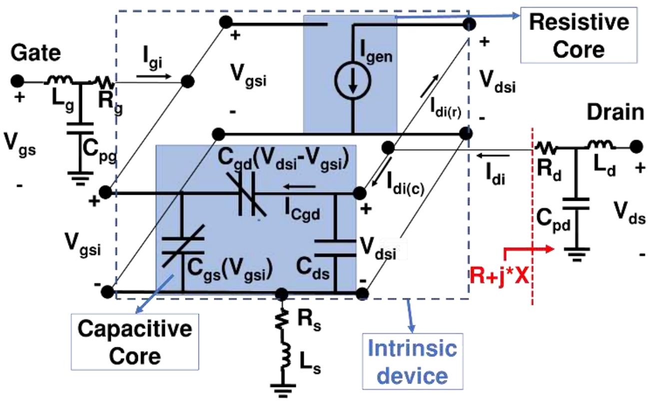

Fig. 1. Equivalent model of a transistor with capacitive and resistive cores; R+j*X denotes the impedance at the fundamental frequency in parallel to Cds.

intrinsic device are calculated as follows:

1. The current from the resistive core ($I_{di(r)}$) and magnitude of the drain voltage in class B (v_s) upon application of a gate voltage (v_{gsi,f_0}) with frequency f_0 is obtained by imposing the loadline on the resistive core[14].
2. The continuum of voltages, V_{dsi}, from Class J* to B to J [12] is calculated using (1)

$$V_{dsi} = V_{dsq} - \delta_J v_s\{\cos(2\pi f_0 t + \Psi_1) + \frac{\alpha}{\sqrt{1+\alpha^2}}\cos(4\pi f_0 t - \frac{\pi}{2})\} \quad (1)$$

Where, $$\delta_J = \sqrt{1+\alpha^2};\ \Psi_1 = \tan^{-1}(\alpha) \quad (2)$$

Where, $\alpha \in [-1,1]$, δ_J denotes the voltage gain over a class B, Ψ_1 denotes the phase of the fundamental component. The values of V_{dsi} obtained from (1) for v_{gsi,f_0}=2V are plotted in Fig. 2 (a).

3. V_{dsi} and V_{gsi} are applied on the capacitive core to obtain the currents through the parasitic components of the intrinsic device. The overall current flowing through the device is obtained by superimposing the currents through the resistive and capacitive cores [14] [16].

Equation (1) reveals that the magnitude and phase of the fundamental frequency increases as we move from class B to J (α=1) and class B to J* (α=-1), as seen in Fig. 2 (a), with classes J/J* having the highest magnitude of the fundamental voltage (δ_J) and phase mismatch (Ψ_1) given by $\sqrt{2}$ and |π/4| respectively. The effect of the magnitude and phase of V_{dsi} on the intrinsic drain current I_{dsi}(=$I_{di(r)}$+I_{Cgd}) where, I_{cgd} denotes the intrinsic capacitive feedback current, is as follows:

(a) Its effect on $I_{di(r)}$ can be ignored if the device is in saturation i.e., the minimum of V_{dsi} remains above the knee voltage (min(V_{dsi})>V_k). The simulated $I_{di(r)}$ is plotted in Fig. 2 (b).

(b) The increase in the magnitude of V_{dsi} with |α| causes the magnitude of I_{Cgd} to increase with |α|, as seen in Fig. 2 (b).

(c) The phase difference between $I_{di(r)}$ and V_{dsi} decreases as α increases (Fig. 2 (a) and (b)). This leads to a reduction of the phase difference between $I_{di(r)}$ and I_{Cgd}, (Fig. 2 (b)), thereby increasing the fundamental component of I_{dsi} ($I_{dsi,f0}$) with α, as shown in Fig. 2 (c). For α=-1, the I_{Cgd} is out of phase with $I_{ds(r)}$, resulting in the lowest drain current through the device.

(a), (b) and (c) are valid if min(V_{dsi})>V_k. Otherwise, strong

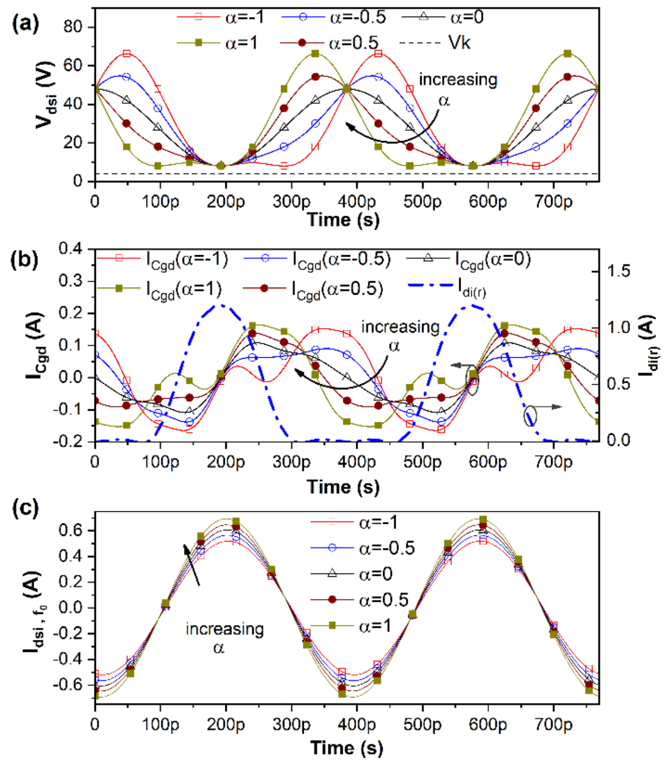

Fig. 2. (a) Intrinsic drain voltage versus time (b) Intrinsic drain current from the resistive core and the feedback capacitor versus time (c) Fundamental component of the intrinsic drain ($I_{dsi,f0}$) current, at Vs=20V and v_{gsi,f_0}=2V for -1≤α ≤1 at a frequency (f_0) of 2.6 GHz and R_L=38.1Ω.

non-linear effects (i.e. clipping of drain current) contribute to the intrinsic drain current. This condition is met only up to a certain amplitude of v_{gsi,f_0} depending on the device and R_L. For the current device and R_L, an amplitude of v_{gsi,f_0}<2.3V satisfies this condition. It can be inferred that as the frequency is varied, the magnitude of I_{Cgd} varies whilst the phase difference between I_{Cgd} and $I_{di(r)}$ remains the same. Hence the difference between the fundamental components of the drain current between α=-1 and α=1 increase with frequency.

B. Influence of Intrinsic Parasitics on Output power, PAE, and IMD3

The output power and PAE are obtained by a procedure, widely used in the literature: The intrinsic impedances at the fundamental ($Z_{L1,int}$) and second harmonic ($Z_{L2,int}$) frequencies of the continuum [12], given by (3), are translated to the extrinsic plane as in [5].

$$Z_{L1,int} = R_L + j\alpha R_L;\ Z_{L2,int} = -j\frac{3\pi}{8}\alpha R_L \quad (3)$$

The optimal source impedance at α=-1 is used for all values of α so that the change in performance of the amplifier (gain, P1dB, and PAE) is a direct consequence of a change in the drain voltage with α. Matching networks are designed using ideal transmission lines.

Due to the increase in drain current with α, the gain of the amplifier and, thereby its efficiency, increase with α as seen from a plot of output power and PAE in Fig. 3 (a). The increase in the gain from α=-1 to 1 is nearly 4dB. Additionally, P1dB of class J is higher than class B whereas the efficiency and P1dB of class J* is less than that of class B. The increase in P1dB is because 1dB compression is determined by harmonics from the

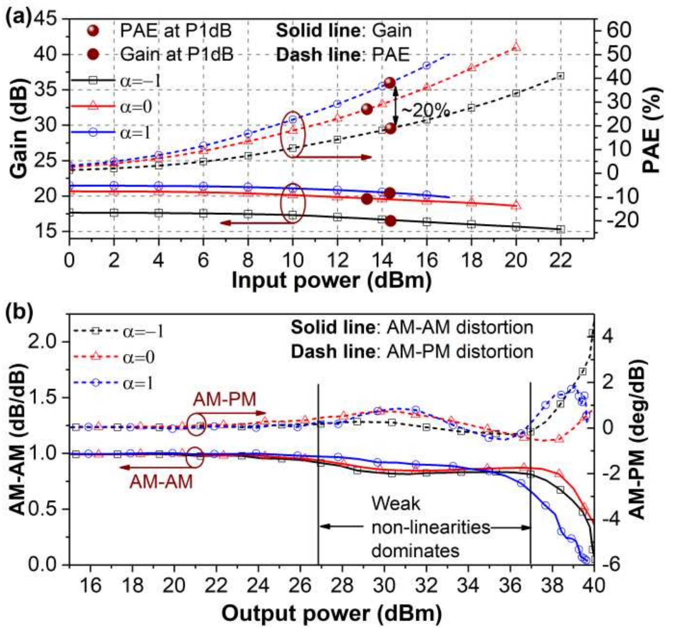

Fig. 3. (a) Gain and PAE as the input power is swept until the minimum of V_{dsi} grazes the knee voltage, and (b) AM/AM and AM/PM distortion. Both simulated at 2.6 GHz for α=-1, 0 and 1 corresponding to classes J*, B and J respectively

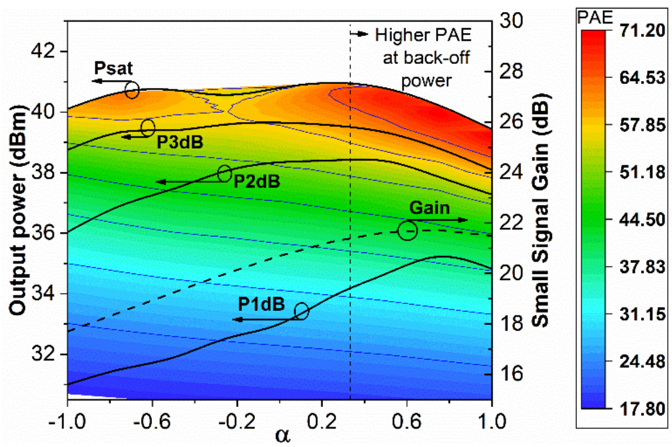

Fig. 4. Simulated P1dB, P2dB, P3dB, Psat (the output power at saturation), and small signal gain for -1≤α ≤1 at 2.6 GHz. Simulated PAE contours as a function of output power and α are overlaid. The corresponding PAE are indicated by colour.

non-linear Cgs and hence achieved at nearly the same input powers for all values of α. Since the gain increases with α, the output power corresponding to 1dB compression (P1dB) increases with α. The increment in P1dB from α=-1 to α=1 is 4dB whereas the increment in PAE corresponding to P1dB (PAE at P1dB) is as high as 20%. These provide significant margins of improvement to amplifier designers.

The additional contribution of I_{Cgd} to the drain current for α=1 leads to a higher change in output power for a given change of input power, than for α=0. Hence AM-AM distortion of class J is lower than for class B (see Fig. 3 (b)). Since the flow of I_{Cgd} is out of phase with respect to I_{dsi} for α=-1 (refer Fig. 2 (b) and (c)), the change of phase with input and hence AM-PM distortion is lower for class J* than for class B, (as shown in Fig. 3 (b)).

The contour plot of PAE with α and output power in Fig. 4 reveals that PAE at back-off output power increases with α, due to the increase in gain with α. The difference in PAE at 5dB back-off output power between classes J* and J is approximately 6%. The variation of P1dB with α is greater than that of P2dB, which is greater than P3dB, as seen in Fig. 4. This is because, at higher compression, non-linear effects due to clipping dominate the performance rather than weak non-linearities. It has been shown that clipping of the drain current causes the output power and PAE of the amplifier to remain constant with α [5]. Consequently, the PAE corresponding to P1dB shows a greater variation than the PAE corresponding to P2dB and P3dB. This observation is in line with literature whereby constant efficiencies over broadband were reported at P2dB [5] or higher compression levels [6], rather than P1dB, while [11] is an exception. In [11], the impedances, which were selected based on extensive load-pull simulations for efficiency near P1dB, in fact, correspond to α>0 (Fig. 4 in [11]) which corroborates the results of this work.

Furthermore, Fig. 4 reveals that the output power decreases for α>0.5 even though the power generated by the intrinsic device increases due to increase in drain current with α. This is because of a reduction of R and |R/X| (to less than 1), given in equation (4), causes the power delivered to the load to reduce as α increases, where R and X (shown in Fig. 1) denote the resistance and reactance respectively in parallel with C_{ds} at the fundamental frequency.

$$R = \frac{R_L}{B^2+(1+\alpha B)^2};\ \frac{R}{X} = \frac{1}{B(1+\alpha^2)+\alpha} \qquad (4)$$

where $B = 2\pi f_0 C_{ds} R_L$.

For B<1, |R/X| becomes less than 1 for $\alpha > \alpha_c$, where,

$$\alpha_c = -\frac{0.5}{B} + \sqrt{\frac{1-4B}{4B^2} - 1} \quad (B < 1) \qquad (5)$$

For the simulation in Fig. 4, B=0.68 and α_c=0.26. Therefore |R/X| gradually decreases from 1 at α=0.26 to 0.5 at α =1 counteracting the increase in power generated at the intrinsic plane due to the feedback capacitor and voltage gain (δ_J). Hence, the maximum output power and small signal gain are achieved at a balance point between α_c and 1, in this case α≈0.65. On the other hand, |R/X|<1 leads to suppression of harmonics of the voltage delivered to the load for $\alpha > \alpha_c$ [17]. With reducing design frequency (i.e. B), α_c increases whereas the effect of parasitics decreases. For low frequencies ($B \ll 1$), leading to $R \approx R_L$ and $|R/X| = |1/\alpha| > 1$, which implies that the power generated at the intrinsic plane is transferred to the load, independent of α. This implies that at high frequencies, where B is close to 1, a subset of the continuum defined by α>α_c has a constant P1dB and a flat gain response.

Simulated third order intermodulation distortion (IMD3) shows small improvement for α>0.5 for P_{out} between 26dBm and 36 dBm, as shown in Fig. 5 (a), because of the lower AM-AM distortion (refer Fig. 3) in this power range, that results in slight improvement in ACPR for average power between 22dBm and 30dBm in Fig. 5 (b). On the other hand, because of the lower AM-PM distortion for α<0, (refer Fig. 3), the EVM (Error Vector Magnitude) improves over class B (Fig. 5 (b)).

The higher gain for α> 0 coupled with slight improvement in IMD3 for P_{out} between 26dBm and 36 dBm, causes PAE corresponding to a given IMD3 (between -30dBc and -20dBc)

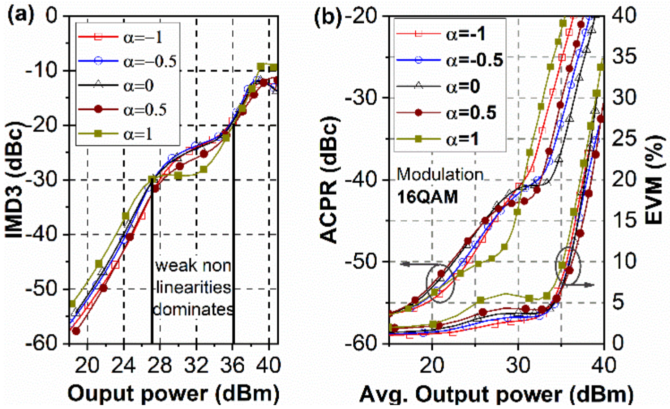

Fig. 5. For -1≤α ≤1, simulated (a) IMD3 versus output power (b) ACPR and EVM versus average output power for a 16-QAM input signal of peak to average ratio 2dB. Data rate (3.84Mbps) and channel bandwidth (5MHz) are same as in WCDMA.

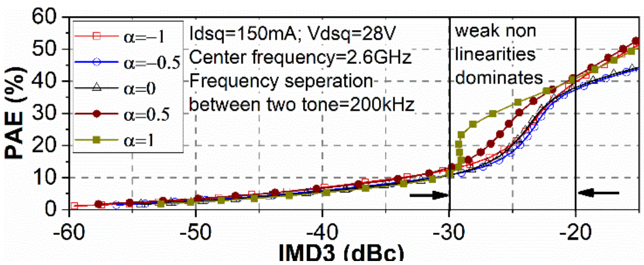

Fig. 6. Simulated PAE versus IMD3 for -1≤α ≤1.

to improve by 10% and 5% for α=1 and α=0.5 respectively as shown in Fig. 6. For lower IMD3 (<-30 dBc), P_{out} <26 dBm, PAE is weakly dependent on α because the drain current is comparable to the bias current and I_{Cgd} is negligible. Importantly, Figures 4, 5, and 6 reveal that for a set of waveforms in the class B/J continuum, higher P1dB, and higher efficiency at P1dB and at back-off power levels is achievable than class B, without sacrificing IMD3. For the current device, operating at frequency 2.6GHz, this set is defined as $\alpha \in [0.4,1]$. The conclusions of this investigation can be extended to continuous class-F which has a similar variation of the phase of voltage [3].

III. Implementation and Experimental Results

A. Amplifier design

Based on Fig. 4 an α≈0.55 is selected as the optimum value for a high P1dB and efficiency at P1dB without sacrificing the maximum output power. The extrinsic fundamental (Z_{L1}) and second harmonic (Z_{L2}) impedances for α≈0.55 are calculated using the method in section II. The optimal source impedance (Z_{s1}) which maximizes P1dB without sacrificing gain, is obtained from source pull simulations of the vendor model. The input and output matching networks are realized using stepped impedance and double stub configurations respectively, as shown in Fig. 7 (a), on a RO4350B substrate of thickness 0.762mm. The output matching network consists of one segment to match Z_{L1} and another segment to match Z_{L2}. A parallel RC network in the input matching network is used to ensure unconditional stability [10]. The designed amplifier is shown in Fig. 7 (b).

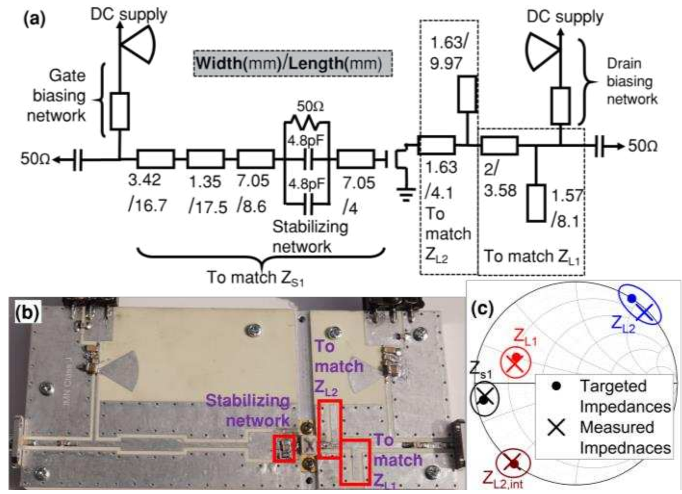

Fig. 7. (a) Schematic of the designed amplifier (b) Photograph of the designed amplifier (c) Measured and targeted source impedances at fundamental frequency (Z_{s1}), extrinsic load impedances at fundamental (Z_{L1}) and second harmonic frequencies (Z_{L2}), and intrinsic load impedances at second harmonic frequency ($Z_{L2,int}$)

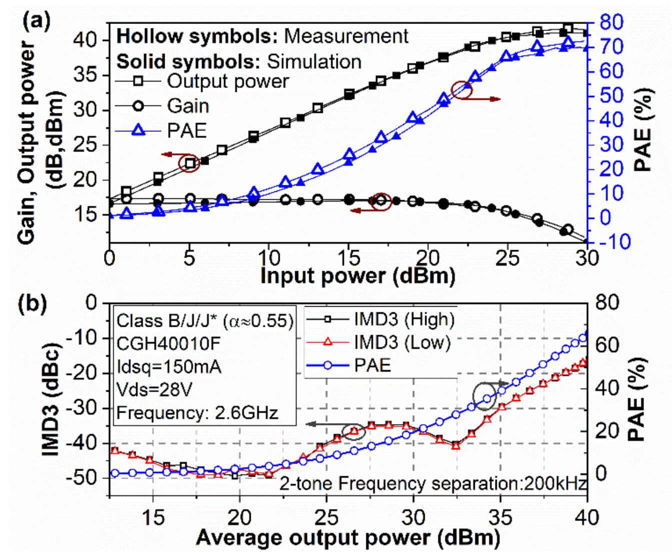

Fig. 8. (a) Measured versus simulated gain, output power and PAE of the designed amplifier. (b) Measured IMD3 and PAE under two-tone excitation centred at 2.6GHz with a frequency separation of 200kHz

B. Measurement Results

The fabricated matching networks are measured individually and compared with target values in Fig. 7 (c), which indicates close agreement for Z_{s1} and Z_{L1}. The difference between the target and measured Z_{L2} does not affect the performance of the amplifier as the discrepancy in the corresponding intrinsic impedances ($Z_{L2,int}$), and in turn, in α, is negligible.

The measured and simulated output power, gain and efficiency of the fabricated class J are plotted in Fig. 8 (a). The peak efficiency achieved is 72.3% and P_{sat} is 41.72dBm. The output power and efficiency at P1dB are 38.13dBm and 54.7% respectively. Measured IMD3 and PAE with a two-tone signal shown in Fig. 8 (b) reveal that IMD3 remains below -30dBc and -20dBc till 35dBm and 38.7dBm output power respectively and attains PAE of 39% and 58.6% respectively.

The designed amplifier is compared with state-of-the-art

TABLE II

STATE OF THE ART HIGH EFFICIENCY LINEAR NARROWBAND AMPLIFIERS USING CGH40010

Ref.	Mode	Freq. (in GHz)	Peak PAE (%)	Figure of Merit	PAE at P1dB (%)	P1dB (dBm)	Psat (dBm)
[8]	Saturated PA	2.14	77.3	113	42.55*	35.06*	40.6*
[10]	Class J	2.13	64.5	94	47.57*	35.73*	39.7
[17]^	Class J	1.5	87#	106#	55.2#	35.6	39.5*
[18]	Class AB	2.25	45	67.5	32	39	40
This work	**Class B/J/J***	**2.6**	**72.3**	**116**	**54.7**	**38.13**	**41.7**

Figure of Merit=Peak PAE*(**Freq.** in GHz)$^{1/2}$ where **Freq.** is Frequency
*Values are extracted from the figures in the papers; ^ design procedure adopted in [24] does not sacrifice efficiency at the reported frequency whilst achieving broad bandwidth; # Drain efficiency

TABLE III

COMPARISON OF ACLR/IMD3 AND AVERAGE PAE WITH NARROWBAND POWER AMPLIFIER USING CGH40010

Reference	Mode	Freq. (GHz)	ACLR/IMD3 (dBc)	Avg. Output power (dBm)	Avg. PAE (%)
[8]	Saturated PA	2.14	-22.3#	34.2	42.3
This work	**Class B/J/J***	**2.6**	**-22.3*#**	**38.25**	**55.8**
[8]	Saturated PA	2.14	-35#	28	20
This work	**Class B/J/J***	**2.6**	**-35*#**	**28**	**17**
[18]	Class AB	2.25	-21	40	41
This work	**Class B/J/J***	**2.6**	**-21**	**38.3**	**56**

Bandwidth of input signal is 10MHz. ACLR in [8] is measured at offset 7.5MHz. * ACLR estimated from measured IMD3 [19] in Fig. 8.

high-efficiency narrowband linear amplifiers using the same device in Table II. Our design shows a higher figure of merit than those reported in terms of output power and PAE at P1dB. The PAE at 5dB back-off is nearly 45%, which is comparable to reported high efficiency at back-off power for the amplifiers with P_{sat} close to 40dBm in Table I. As can be seen from Fig. 4, an even higher efficiency can be achieved by choosing a higher value of α but at the expense of output power and P1dB. A comparison of the fabricated PA with saturated PA, optimized for peak efficiency from [8], in Table III reveals that the designed amplifier achieves PAE lower by 3% at -35dBc ACLR whereas 13% higher PAE is achieved at ACLR of -22.3 dBc than the saturated PA. The designed amplifier achieves 14% higher PAE than class AB at the same IMD3 level as in [18]. This shows that higher efficiencies than class AB and saturated PA can be achieved for a given distortion in the region dominated by the effect of non-linear capacitances, for this device between -30dBc and -20dBc.

IV. CONCLUSIONS

A study of the non-linear feedback capacitance shows that the gain, P1dB, and efficiency at back-off power of an amplifier increase from class J* to class B to class J. This can be attributed to a variation of the phase of the voltage waveforms across its non-linear Cgd. Based on this knowledge, the trade-off involved with alpha are analyzed in this brief. It is shown that a subset of the continuum results in higher PAE at P1dB than Class B (or deep class AB) and these modes can be replaced by the class B/J/J*, at a higher frequency, without sacrificing linearity using the methodology presented here. This brief utilizes this hitherto unknown benefit of a remarkable 20% increase in efficiency at P1dB from class J* to J, to demonstrate a prototype amplifier with 72% PAE, 38 dBm P1dB and 55% PAE at P1dB.

V. REFERENCES

[1] S. C. Cripps, P. J. Tasker, A. L. Clarke, J. Lees, and J. Benedikt, “On the continuity of high efficiency modes in linear RF power amplifiers,” IEEE Microw. Wirel. Components Lett., vol. 19, no. 10, pp. 665–667, 2009.

[2] M. Ozen, R. Jos, and C. Fager, “Continuous class-e power amplifier modes,” IEEE Trans. Circuits Syst. II Express Briefs, vol. 59, no. 11, pp. 731–735, 2012.

[3] V. Carrubba, A. L. Clarke, M. Akmal, J. Lees, J. Benedikt, P. J. Tasker, and S. C. Cripps, “On the extension of the continuous class-F mode power amplifier,” IEEE Trans. Microw. Theory Tech., vol. 59, no. 5, pp. 1294–1303, 2011.

[4] T. Sharma, R. Darraji, and F. Ghannouchi, “A Methodology for Implementation of High Efficiency Broadband Power Amplifiers with Second Harmonic Manipulation,” IEEE Trans. Circuits Syst. II Express Briefs, vol. 63, no. 1, pp. 1–1, 2015.

[5] P. Wright, J. Lees, J. Benedikt, P. J. Tasker, and S. C. Cripps, “A methodology for realizing high efficiency class-J in a Linear and Broadband PA,” IEEE Trans. Microw. Theory Tech., vol. 57, no. 12, pp. 3196–3204, 2009.

[6] S. Saxena, K. Rawat, and P. Roblin, “Continuous Class-B/J Power Amplifier Using Nonlinear Embedding Technique,” IEEE Trans. Circuits Syst. II Express Briefs, vol. 1, no. 1, pp. 1–1, 2016.

[7] K. Mimis, K. A. Morris, S. Bensmida, and J. P. McGeehan, “Multichannel and wideband power amplifier design methodology for 4G communication systems based on hybrid class-J operation,” IEEE Trans. Microw. Theory Tech., vol. 60, no. 8, pp. 2562–2570, 2012.

[8] J. Moon, J. Kim, and B. Kim, “Investigation of a class-J power amplifier with a nonlinear Cout for optimized operation,” IEEE Trans. Microw. Theory Tech., vol. 58, no. 11 PART 1, pp. 2800–2811, 2010.

[9] A. Alizadeh and A. Medi, “A Broadband Integrated Class-J Power Amplifier in GaAs pHEMT Technology,” IEEE Trans. Microw. Theory Tech., vol. 64, no. 6, pp. 1–9, 2016.

[10] K. Mimis, K. A. Morris, and J. P. McGeehan, “A 2GHz GaN Class-J power amplifier for base station applications,” in IEEE Topical Conference on Power Amplifiers for Wireless and Radio Applications (PAWR), 2011, pp. 5–8.

[11] R. Ma, S. Goswami, K. Yamanaka, Y. Komatsuzaki, and A. Ohta, “A 40-dBm high voltage broadband GaN Class-J power amplifier for PoE micro-basestations,” IEEE MTT-S Int. Microw. Symp. Dig., pp. 30–32, 2013.

[12] S. Rezaei, L. Belostotski, F. M. Ghannouchi, and P. Aflaki, “Integrated design of a class-J power amplifier,” IEEE Trans. Microw. Theory Tech., vol. 61, no. 4, pp. 1639–1648, 2013.

[13] N. Tuffy, L. Guan, A. Zhu, and T. J. Brazil, “A simplified broadband design methodology for linearized high-efficiency continuous class-F power amplifiers,” IEEE Trans. Microw. Theory Tech., vol. 60, no. 6 PART 2, pp. 1952–1963, 2012.

[14] M. Rasheduzzaman, “Contributing Towards Improved Communications Systems for Future Cellular Networks,” PhD thesis, Department of Electronic and Electrical Engineering, University of Sheffield, 2016.

[15] J. A. Z. Flores, “Device Characterization and Modeling of Large-Size GaN HEMTs,” PhD thesis, Department of Electrical Engineering and Computer Science, University of Kassel, Germany, 2012.

[16] A. Raffo, F. Scappaviva, and G. Vannini, “A New Approach to Microwave Power Amplifier Design Based on the Experimental Characterization of the Intrinsic Electron-Device Load Line,” IEEE Trans. Microw. Theory Tech., vol. 57, no. 7, pp. 1743–1752, 2009.

[17] B. Bukvi and M. I. Milan, “Simple Design of a Class-J Amplifier With Predetermined Efficiency,” IEEE Microw. Wirel. Components Lett., vol. 26, no. 9, pp. 699–701, 2016.

[18] T. Khan and U. Naeem, “10W Power-amplifier design based on passive Load pull,” in 17th IEEE International Multi Topic Conference, 2014, pp. 519–522.

[19] N. B. Carvalho and J. C. Pedro, “Multi-Tone Intermodulation Distortion Performance of 3rd Order Microwave Circuits,” IEEE MTT-S Int. Microw. Symp. Dig., vol. 2, pp. 763–766, 1999.